Potential barriers governing the 12C formation and decay through quasimolecular shapes

Guy Royer, Antony Escudie, B. Sublard

PHYSICAL REVIEW C 00, 004600 (2014)

Potential barriers governing the ^{12}C formation and decay through quasimolecular shapes

G. Royer, A. Escudie, and B. Sublard
Laboratoire Subatech, UMR: IN2P3/CNRS-Université-Ecole des Mines, Nantes 44, France
(Received 10 February 2014; revised manuscript received 18 June 2014; published xxxxxx)

The L dependent potential barriers that govern the ^{8}Be and ^{12}C formation and decay through quasimolecular shapes have been determined using a generalized liquid-drop model and adjusted to reproduce the experimental Q value. For the ternary channel of ^{12}C, the energies of prolate linear chain configurations and oblate triangular configurations of three α particles have been compared. The triangular shape with three α nuclei in contact allows the experimental rms radius and the negative quadrupole moment of the ^{12}C ground state to be reproduced. The difference between the energies of the minima in the prolate and oblate ternary shape paths are very close to the energy of the excited Hoyle state of the ^{12}C nucleus.

DOI: 10.1103/PhysRevC.00.004600 PACS number(s): 26.20.Fj, 25.60.Pj, 21.60.Ev, 21.10.−k

I. INTRODUCTION

Hydrogen burning in stars leads to a dense and hot core of helium that fuels the nucleosynthesis of the heavier elements. The "triple-α" capture phenomenon has been advanced to explain the formation of the ^{12}C nuclei. In a first stage of this process two α particles resonate in the ground state of ^{8}Be. The half-life of this state (8.2×10^{-17}s) allows the capture of a third particle before it disintegrates leading to the 0_2^+ excited Hoyle state of ^{12}C ($E^* = 7.6542$ MeV). The probability of such a process is non-negligible because this excitation energy is very close to the $Q_{\alpha+^{8}\mathrm{Be}} = 7.3666$ MeV and $Q_{3\alpha} = 7.2747$ MeV thresholds. The knowledge of the shape of the ^{12}C nucleus in its ground and excited states is of great importance to fully understand this fusion reaction.

Theoretically, after calculating transition densities derived from the three-α resonating-group wave functions it was concluded that the shape of the ground state of ^{12}C is oblate [1]. Within an isomorphic shell model it has been assumed that both the ground state and the first 0^+ excited state can be associated with an α chain composed of three particles in a row [2], but the decay width of the Hoyle state is not reproduced. Calculations using antisymmetrized molecular dynamics and Fermionic molecular dynamics without assuming α clustering have allowed the low-lying spectrum of ^{12}C to be reproduced [3,4]. It has also been found that the 0_2^+ Hoyle state has a Bose-Einstein dilute 3α condensatelike structure [5,6]. Recent *ab initio* lattice calculations have led to a compact triangular configuration for the ^{12}C ground state and the first excited state 2_1^+ state and to a "bent-arm" or obtuse triangular configuration of α clusters for the Hoyle state and the second excited 2_2^+ state [7]. The no core shell model has shown that the collective states and states with clusterlike substructures can emerge out of a fully microscopic shell model framework [8]. The Hoyle state has also been described in terms of a local potential $^{8}\mathrm{Be} + \alpha$ cluster model [9].

Experimentally, the value of the root-mean-square charge radius of the ground state of ^{12}C is $\langle r^2 \rangle^{1/2} = 2.47$ fm [10]. The electric quadrupole moment of the ^{12}C ground state is $Q_0 = -22^{+}_{-}10$ e fm^2 assuming that the nuclear charge distribution is spheroidal with $K = 0$ [11], which indicates a substantial oblate deformation incompatible with the linear chain configuration of three α particles. To populate the Hoyle state of ^{12}C [12,13] fragmentation of quasiprojectiles in the reaction $^{40}\mathrm{Ca} + ^{12}\mathrm{C}$ at 25 MeV/nucleon was employed; $7.5 \pm 4\%$ of the particle decays of the Hoyle state correspond to direct decays in three equal-energy α particles and thus fulfill the decay criteria of an α-particle condensate. Moreover, events with increased kinetic energy dispersion in the ^{12}C center of mass, which amount to $9.5 \pm 4\%$, point toward the occurrence of a second molecular configuration, a linear α-chain type. Different ratios have also been provided [14]. Beyond the excited 0_2^+ Hoyle state, evidence has been observed for a possible 2^+ state at 9.6(1) MeV with a width of 600(100) keV [15]. Analyzing (α,α') cross-section data, a 2^+ excitation of the Hoyle state and the α-condensate state at $E_x = 9.84 \pm 0.06$ MeV with a width of 1.01 ± 0.15 MeV have also been found [16].

The purpose of this work is to determine the L-dependent potential barriers governing the evolution of the ^{8}Be nucleus of the $^{8}\mathrm{Be} + ^{4}\mathrm{He}$ system and the $^{4}\mathrm{He} + ^{4}\mathrm{He} + ^{4}\mathrm{He}$ oblate triangular and prolate longitudinal configurations in the framework of a generalized liquid-drop model (GLDM)and of binary and ternary quasimolecular shapes.

II. GENERALIZED LIQUID-DROP MODEL

This version of the liquid-drop model has been used previously to determine the fusion barriers and cross sections [17,18], the binary [19] and ternary [20] fission barriers and characteristics, and the α-decay potential barriers and half-lives [21].

The GLDM energy is the sum of the volume, surface, Coulomb, and nuclear proximity energies. For a one-body shape nucleus, the first three contributions are given by

$$E_V = -15.494(1 - 1.8I^2)A \text{ MeV}, \quad (1)$$

$$E_S = 17.9439(1 - 2.6I^2)A^{2/3}\frac{S}{4\pi R_0^2} \text{ MeV}, \quad (2)$$

where $I = (N - Z)/A$ is the relative neutron excess and S is the surface of the deformed nucleus, and

$$E_C = 0.6e^2(Z^2/R_0)B_C. \quad (3)$$

The Coulomb-shape-dependent function B_C is expressed as

$$B_C = \frac{15}{16\pi^2 R_0^5} \int d\tau \int \frac{d\tau'}{|r - r'|}. \quad (4)$$

By using the axial symmetry of the system and complete elliptic integrals it reduces to

$$B_C = 0.5 \int (V(\theta)/V_0)(R(\theta)/R_0)^3 \sin\theta d\theta. \quad (5)$$

$V(\theta)$ is the electrostatic potential at the surface and V_0 is the surface potential of the sphere. The nuclear radius is defined as

$$R_0 = (1.28A^{1/3} - 0.76 + 0.8A^{-1/3})\ \text{fm}. \quad (6)$$

This formula was derived from the droplet model and from the proximity energy values.

All along the entrance or decay channels the proximity energy term takes into account the effects of the nuclear attractive forces between nucleons being studied in a neck, in the case of a deformed one-body shape or across the gap and in the case of two or three nuclei. This is an additional term to the surface energy which takes into account only the effects of the nuclear forces in a half-space. This proximity term is necessary to reproduce the fusion barrier heights, beyond the pure Coulomb peak approximation. It is particularly important when there are two or three spherical nuclei in contact and for quasimolecular one-body shapes where the necks are narrow and well developed. When the proximity energy is taken into account, the potential barrier is smooth even at the contact point and the top of the barrier corresponds to separated nuclei maintained in unstable equilibrium by the balance between the repulsive Coulomb forces and the attractive nuclear proximity forces. As examples, the symmetric fission barrier of a ^{234}U nucleus through compact and creviced shapes is lowered by around 40 MeV by the proximity energy [22,23] and then the barrier height is comparable to the experimental data. The proximity forces lower of 5.7 MeV the barrier against α emission from a ^{264}Hs nucleus, the displacement of the barrier top to a more external position being of 2.1 fm [21].

The proximity energy reads

$$E_{\text{prox}}(r) = 2\gamma \int \Phi\,[D(r,h)/b]\, 2\pi h dh, \quad (7)$$

where r is the distance between the mass centers, Φ is the proximity function of Feldmeier [24], h is the transverse distance varying from the neck radius for one-body shapes and zero for separated nuclei to the height of the neck border, b is the surface width ($b = 0.99$ fm), D is the distance between the opposite surfaces on a line parallel to the separation axis (see Ref. [17]), and γ is the surface parameter:

$$\gamma = 0.9517(1 - k_s I^2)\ \text{MeV fm}^{-2}. \quad (8)$$

The experimental Q value which incorporates the microscopic corrections plays a main role. It has been taken into account empirically in adding the difference between the experimental and the theoretical Q values deduced from the GLDM at the macroscopic potential energy of the mother spherical nucleus with a linear attenuation factor vanishing at the contact point of the two or three fragments or incoming nuclei.

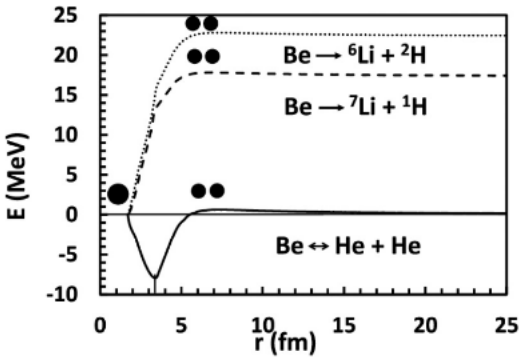

FIG. 1. Potential barriers governing the $^8\text{Be} \leftrightarrow {}^4\text{He} + {}^4\text{He}$, $^8\text{Be} \rightarrow {}^7\text{Li} + {}^1\text{H}$, and $^8\text{Be} \rightarrow {}^6\text{Li} + {}^2\text{H}$ reactions versus the distance between the mass centers (at $L = 0$). The vertical dash indicates the contact point between the two nuclei.

To describe the evolution of one sphere to two spheres in contact assuming volume conservation, elliptic lemniscatoids have been retained because they allow the progressive formation of a deep neck while keeping almost spherical ends [17]. A generalization of this shape sequence permits one to also describe the prolate ternary path that leads from a sphere to three aligned spheres in contact [20] and then to simulate the linear chain configurations of three α particles. The oblate ternary fission or fusion has been described from the contact point between three α particles arranged on an equilateral triangle and which separate in keeping the same triangular configuration [25]. The proximity energy is maximized for such shape sequences.

III. ^{8}Be NUCLEUS

First, the ^{8}Be nucleus is considered. The potential barriers of the three reactions $^8\text{Be} \leftrightarrow {}^4\text{He} + {}^4\text{He}$, $^8\text{Be} \leftrightarrow {}^7\text{Li} + {}^1\text{H}$, and $^8\text{Be} \leftrightarrow {}^6\text{Li} + {}^2\text{H}$ are displayed in Fig. 1 and the characteristics are given in Table I. The figure displays the deformation

TABLE I. Characteristics of different ^{8}Be entrance or decay channels. r_{sph} and r_{cont} are, respectively, the distance between the mass centers of the two parts of the system at the sphere and at the contact point while $r_{E_{\min}}$ and $r_{E_{\max}}$ indicate the position of the minimum and maximum of the potential barriers.

	r_{sph}	$r_{E_{\min}}$	r_{cont}	$r_{E_{\max}}$	∞
$^8\text{Be} \leftrightarrow {}^4\text{He} + {}^4\text{He}$					
r (fm)	1.65	3.39	3.49	7.45	
E (MeV)	0	−7.95	−7.84	0.62	−0.0918
$^8\text{Be} \rightarrow {}^7\text{Li} + {}^1\text{H}$					
r (fm)	1.73		3.33	6.89	
E (MeV)	0		12.94	17.82	17.25
$^8\text{Be} \rightarrow {}^6\text{Li} + {}^2\text{H}$					
r (fm)	1.69		3.42	7.38	
E (MeV)	0		15.43	22.81	22.28

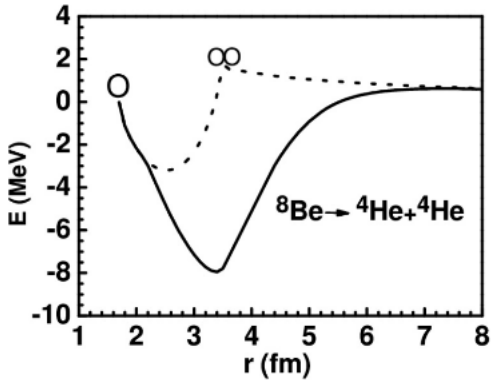

FIG. 2. Comparison between the deformation energies calculated without (broken curve) and with (full curve) a proximity energy term for the ^{8}Be ↔ ^{4}He + ^{4}He reaction.

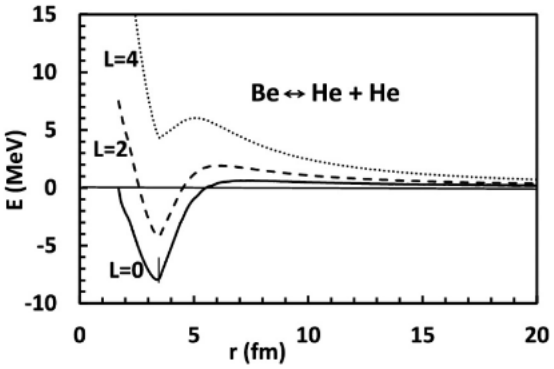

FIG. 3. Potential barriers of the ^{8}Be ↔ ^{4}He + ^{4}He reaction as a function of the angular momentum (in $\hbar$ units).

energy relatively to the sphere energy, which explains that the potential barriers start from the same energy point. For the largest deformations the energy corresponds to the Q value of the fusion process. The top of the barriers corresponds to two separated spheres. The possibility of resonant states exists in the ^{4}He + ^{4}He channel.

The influence of the proximity energy term is underlined in Fig. 2. The unrealistic pure Coulomb peak is given by the dashed curve. The maximum corresponds to the contact point. When the effects of the proximity forces are taken into account the energy at the contact point diminishes by around 9.4 MeV while the barrier top is shifted 4 fm.

Within this macroscopic model the decay constant is simply given by $\lambda = \nu_0 P$. The assault frequency ν_0 has been taken as $\nu_0 = 10^{20}$ s^{-1}. The barrier penetrability P is calculated within the action integral:

$$P = \exp\left[-\frac{2}{\hbar}\int_{r_{\rm in}}^{r_{\rm out}} \sqrt{2B(r)[E(r) - E_{\rm g.s.}]}dr\right]. \qquad (9)$$

The inertia $B(r)$ is related to the reduced mass by

$$B(r) = \mu\{1 + 24\exp[-3.25(r - R_{\rm sph})/R_0]\}, \qquad (10)$$

where $R_{\rm sph}$ is the distance between the mass centers of the future fragments in the initial sphere; $R_{\rm sph}/R_0 = 0.75$ in the symmetric case. For shapes near the ground state the inertia is largely above the irrotational flow value because a large amount of internal reorganization occurs at level crossings. For highly deformed shapes the reduced mass is reached asymptotically. Such a prescription for the inertia parameter has allowed the fission half-lives of the actinide nuclei to be precisely reproduced [19]. A more detailed discussion of this parameter may be found in Ref. [26].

The partial half-life is finally obtained by $T_{1/2} = \frac{\ln 2}{\lambda}$. Here, the instability of the ^{8}Be nucleus against its symmetric decay leads to a theoretical half-life of 5.7×10^{-16} s, a value close to the experimental value 8.2×10^{-17} s. The rotational energy is given by

$$E_{\rm rot} = \hbar^2 l(l+1)/2J, \qquad (11)$$

assuming a rigid moment of inertia. The L-dependent barriers are displayed in Fig. 3. The indicated energy is the sum of the deformation energy and of the rotational energy. The theoretical energies of the 2 and 4 states are, respectively, 3.78 and 12.25 MeV, not too far from the experimental values, 3.03 and 11.35 MeV, of the energies of the 2^+ and 4^+ states. Nevertheless, this potential does not allow us to reproduce the half-life for the $L = 2$ level.

IV. ^{12}C NUCLEUS

Several binary channels governing the ^{12}C evolution are compared in Fig. 4 and the characteristics are given in Table II. The respective Q values are −7.365, −25.19, −26.28, and −28.17 MeV. Resonant states are possible in the very specific ^{12}C ↔ ^{8}Be + ^{4}He channel. They correspond to a quasimolecular one-body shape formed by two nuclei connected by a narrow neck.

The potential barriers corresponding to the direct aligned 3α fusion and the ^{8}Be + ^{4}He fusion reaction are compared in Fig. 5. The Q values are almost identical, respectively, 7.2747 and 7.3666 MeV. The proximity energy between three aligned α particles is stronger than the proximity energy between an assumed spherical ^{8}Be nucleus and an α particle because there are two necks for the ternary configuration. The proximity forces act at larger values of the distance r in the ternary case, which explains the crossing of the curves at $r = 8$ fm.

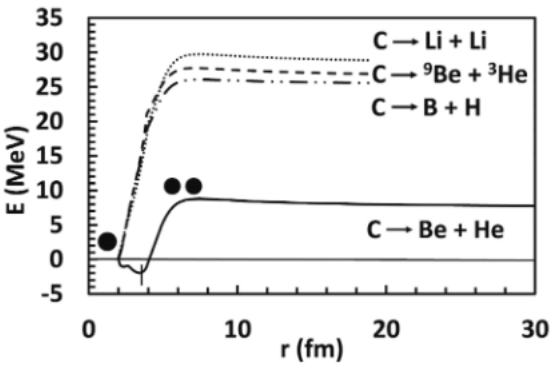

FIG. 4. Potential barriers governing the ^{12}C ↔ ^{8}Be + ^{4}He, ^{12}C → ^{10}B + ^{2}H, ^{12}C → ^{9}Be + ^{3}He, and ^{12}C → ^{6}Li + ^{6}Li reactions versus the distance between the mass centers (at $L = 0$). The vertical dash indicates the contact point between the two nuclei.

TABLE II. Same as Table I but for the ^{12}C nucleus reactions.

	r_{sph}	$r_{E_{min}}$	r_{cont}	$r_{E_{max}}$	∞
$^{12}C \leftrightarrow {}^{8}Be + {}^{4}He$					
r (fm)	1.91	3.41	3.96	7.43	
E (MeV)	0.00	−1.95	−0.63	8.77	7.365
	r_{cms}		r_{cmc}	$r_{E_{max}}$	∞
$^{12}C \rightarrow {}^{10}B + {}^{2}H$					
r (fm)	1.98		3.81	7.49	
E (MeV)	0.00		18.26	26.06	25.19
$^{12}C \rightarrow {}^{9}Be + {}^{3}He$					
r (fm)	1.94		3.90	7.12	
E (MeV)	0.00		20.97	27.73	26.28
$^{12}C \rightarrow {}^{6}Li + {}^{6}Li$					
r (fm)	1.89		4.0	7.48	
E (MeV)	0.00		19.63	29.44	28.17

The L-dependent potential barriers in the prolate ternary shape path are shown in Fig. 6. A minimum persists even at relatively high angular momenta.

Experimentally, the value of the electric quadrupole moment of the ^{12}C ground state is $Q_0 = -22 \pm 10$ e fm^2 assuming that the nuclear charge distribution is spheroidal with $K = 0$ [11], which indicates a substantial oblate deformation incompatible with the linear chain configuration of three α particles. The other fundamental property is the root-mean-square charge radius $\langle r^2 \rangle^{1/2} = 2.47$ fm for the ^{12}C nucleus [10].

To study these oblate ternary configurations three spherical α particles have been placed in contact on an equilateral triangle (see Fig. 7) and later separated and moved away from each other in keeping the regular triangular configuration. At the contact point, the rms radius is $\langle r^2 \rangle^{1/2} = 2.43$ fm and the electric quadrupole moment is $Q_0 = -24.4\, e$ fm^2, both in very good agreement with the experimental data.

All along the deformation path the rms radius is connected with the distance l from the center of each fragment to the mass center of the total system by [25]

$$\langle r^2 \rangle = \tfrac{3}{5} R_0^2 3^{-2/3} + l^2. \quad (12)$$

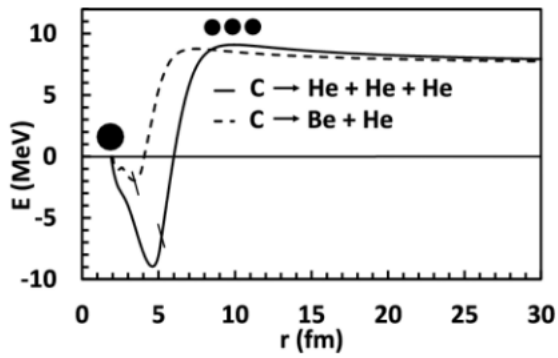

FIG. 5. Comparison between the potential barriers governing the $^{12}C \leftrightarrow {}^{8}Be + {}^{4}He$ and $^{12}C \leftrightarrow {}^{4}He + {}^{4}He + {}^{4}He$ binary and prolate ternary reactions.

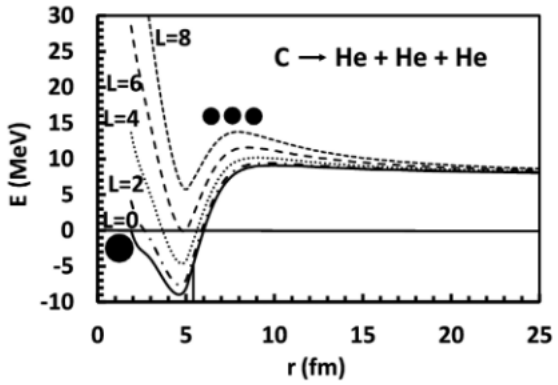

FIG. 6. Potential barriers of the $^{12}C \leftrightarrow {}^{4}He + {}^{4}He + {}^{4}He$ reaction as a function of the angular momentum and for a linear chain configuration.

The L-dependent potential barriers seen by this oblate configuration of three α particles are displayed in Fig. 8. For such a shape the proximity energy between the nucleons under study is very important; $E_{prox} = -28.2$ MeV at the contact point. For the linear chain, there are only two necks and the proximity energy is only −18.8 MeV at the touching point. Therefore the characteristics of the oblate configuration of three α particles in contact at the top of an equilateral triangle seem compatible with the experimental data available on the ground state of the ^{12}C nucleus. Furthermore the difference between the energy of the minima of the potential barrier of the 3α linear chain and the minima of the oblate equilateral configuration is 7.36 MeV, a value very close to the energy of the excited Hoyle state. This is in favor of a linear chain configuration for the Hoyle state. Then the $L = 2$ and $L = 4$ excited states of the prolate longitudinal chain have energies of, respectively, 8.7 and 11.7 MeV compared with the experimental value of the 2^+ state at 9.6(1) MeV with a width of 600(100) keV [15].

The feasibility of such a liquid-drop approach for such light systems is evidently questionable. At least, one may be confident with the calculation of the proximity energy because it allows one to reproduce precisely the fusion barrier heights and positions of symmetric and very asymmetric light systems such as $^{9}Be + {}^{10}B$, $^{4}He + {}^{44}Ca$, $^{4}He + {}^{233}U$ [27] and also to

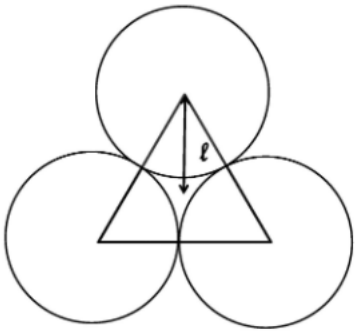

FIG. 7. Oblate ternary configuration of three α particles in contact. l is the distance between the mass center of an α particle and the mass center of the whole system.

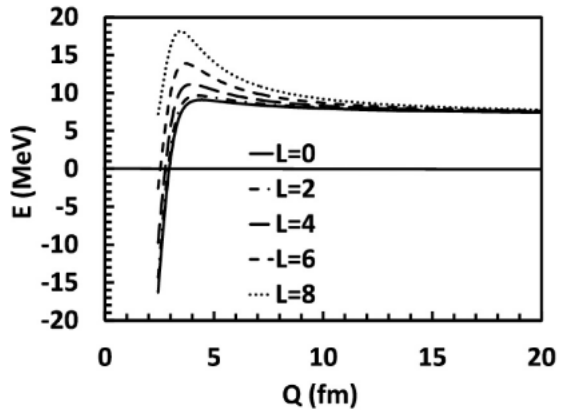

FIG. 8. L-dependent potential barriers for the $^{12}C \leftrightarrow {}^{4}He + {}^{4}He + {}^{4}He$ reaction and a triangular configuration. Q is the rms radius.

determine precisely the α-decay potential barriers [21] with the help of the experimental Q value. One may also wonder that such a liquid-drop model is available (when taking also into account other terms) to reproduce the mass of light nuclei even though the accuracy is lower than that for heavier nuclei [28]. Another open question is the availability of such an approach for such distorted quasimolecular or two-body and three-body shapes. The question is the same for microscopic theories using mean fields.

As stated in the Introduction, much more elaborated microscopic quantum theories have been developed recently. They allow one to determine accurate density profiles and, in particular, to obtain one-body "bent-arm" or obtuse triangular configurations. The reproduction of the transition from one-body to two- or three-body shapes or the fusion process is more difficult and time-consuming.

V. SUMMARY AND CONCLUSION

In conclusion, within a GLDM taking into account the proximity energy and adjusted to reproduce the experimental Q value, the L-dependent potential barriers for the binary $^{12}C \leftrightarrow {}^{8}Be + {}^{4}He$ and $^{12}C \leftrightarrow {}^{4}He + {}^{4}He + {}^{4}He$ prolate and oblate ternary reactions have been calculated. The oblate triangular configuration of three α particles in contact is compatible with the experimental rms radius and electric quadrupole moment while the linear configuration of three aligned α particles allows one to reproduce roughly the energy of the excited 0^+ Hoyle state and the energy of the excited 2^+ Hoyle state.

[1] M. Kamimura, Nucl. Phys. A **351**, 456 (1981).
[2] G. S. Anagnostatos, Phys. Rev. C **51**, 152 (1995).
[3] Y. Kanada-En'yo, Prog. Theor. Phys. **117**, 655 (2007).
[4] M. Chernykh, H. Feldmeier, T. Neff, P. von Neumann-Cosel, and A. Richter, Phys. Rev. Lett. **98**, 032501 (2007).
[5] T. Yamada and P. Schuck, Eur. Phys. J. A **26**, 185 (2005).
[6] H. Horiuchi, in *Proceedings of the 13th International Conference on Nuclear Reaction Mechanisms*, edited by F. Cerutti *et al.* (CERN Proceedings-2012-002), p. 261.
[7] E. Epelbaum, H. Krebs, T. A. Lähde, D. Lee, and Ulf-G. Meissner, Phys. Rev. Lett. **109**, 252501 (2012).
[8] A. C. Dreyfuss, K. D. Launey, T. Dytrych, J. P. Draayer, and C. Bahri, Phys. Lett. B **727**, 511 (2013).
[9] B. Buck, A. C. Merchant, and S. M. Perez, Phys. Rev. C **87**, 024304 (2013).
[10] I. Angeli, At. Data Nucl. Data Tables **87**, 185 (2004).
[11] W. J. Vermeer *et al.*, Phys. Lett. B **122**, 23 (1983).
[12] A. R. Raduta *et al.*, Phys. Lett. B **705**, 65 (2011).
[13] A. R. Raduta *et al.*, J. Phys.: Conf. Ser. **420**, 012087 (2013).
[14] T. K. Rana *et al.*, Phys. Rev. C **88**, 021601(R) (2013).
[15] M. Freer *et al.*, Phys. Rev. C **80**, 041303(R) (2009).
[16] M. Itoh *et al.*, Phys. Rev. C **84**, 054308 (2011).
[17] G. Royer and B. Remaud, Nucl. Phys. A **444**, 477 (1985).
[18] G. Royer and J. Gaudillot, Phys. Rev. C **84**, 044602 (2011).
[19] G. Royer, M. Jaffré, and D. Moreau, Phys. Rev. C **86**, 044326 (2012).
[20] J. Mignen and G. Royer, J. Phys. G: Nucl. Phys. **13**, 987 (1987).
[21] G. Royer, J. Phys. G: Nucl. Part. Phys. **26**, 1149 (2000).
[22] G. Royer and B. Remaud, J. Phys. G: Nucl. Phys. **10**, 1057 (1984).
[23] G. Royer, *Heavy Elements and Related New Phenomena* (World Scientific, Singapore, 1999).
[24] H. Feldmeier, in *Proceedings of the 12th Summer School on Nuclear Physics*, Mikolajki, Poland, 1979.
[25] G. Royer and F. Haddad, J. Phys. G: Nucl. Part. Phys. **20**, L131 (1994).
[26] P. Möller, J. R. Nix, and W. J. Swiatecki, Nucl. Phys. A **492**, 349 (1989).
[27] G. Royer, J. Phys. G: Nucl. Phys. **12**, 623 (1986).
[28] G. Royer and A. Subercaze, Nucl. Phys. A **917**, 1 (2013).